

1 **Diammonium hydrogenphosphate for the consolidation of building materials.**

2 **Investigation of newly-formed calcium phosphates**

3

4 Elena Possenti,^{a, b} * Chiara Colombo,^b Claudia Conti,^b Lara Gigli,^c Marco Merlini,^a Jasper
5 Rikkert Plaisier,^c Marco Realini,^b Diego Sali^d, G. Diego Gatta^a

6 ^a*Dipartimento di Scienze della Terra, Università degli Studi di Milano, Via Botticelli 23, 20133 Milan, Italy*

7 ^b*Istituto per la Conservazione e la Valorizzazione dei Beni Culturali (ICVBC), Consiglio Nazionale delle*
8 *Ricerche (CNR), Via R. Cozzi 53, 20125 Milan, Italy*

9 ^c*Elettra - Sincrotrone Trieste S.c.P.A., strada statale 14, 34149 Basovizza, Trieste, Italy*

10 ^d*Bruker Italia S.r.l. Unipersonale, V. le V. Lancetti 43, 20158, Milan, Italy*

11 * *Corresponding author: possenti@icvbc.cnr.it, Phone number: +39 02 66173386*

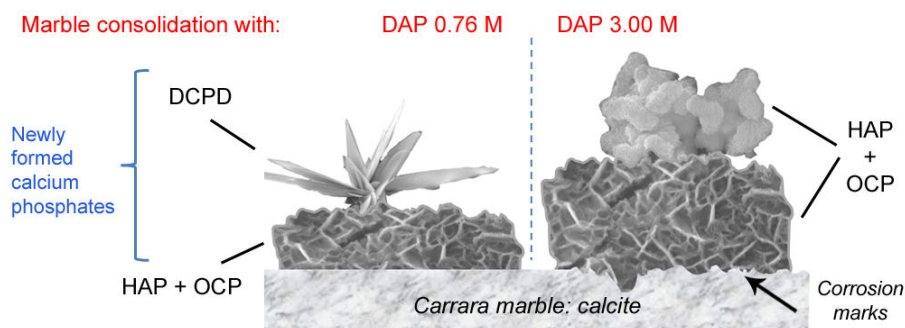
12 *E-mail addresses: possenti@icvbc.cnr.it (E. Possenti), c.colombo@icvbc.cnr.it (C. Colombo),*
13 *c.conti@icvbc.cnr.it (C. Conti), diego.gatta@unimi.it (G. D. Gatta), lara.gigli@elettra.eu (L. Gigli),*
14 *marco.merlini@unimi.it (M. Merlini), jasper.plaisier@elettra.eu (J. R. Plaisier), m.realini@icvbc.cnr.it (M.*
15 *Realini), diego.sali@bruker.com (D. Sali)*

16 **Declarations of interest:** none

17 **Highlights**

- 18 • Diammonium hydrogenphosphate (DAP) solutions consolidate decayed carbonatic stones
- 19 • The formed phases depend on treatment method, DAP molarity and stone microstructure
- 20 • Cutting-edge techniques are discussed to identify similar crystalline phases
- 21 • The formation of hydroxyapatite is unambiguously demonstrated
- 22 • Variables which might affect the treatment effectiveness are discussed

23 **Graphical abstract**



24

25 The graphical abstract and all the figures can be printed in black and white

26

27 **Abstract**

28 Diammonium hydrogenphosphate (DAP) is a water soluble consolidant for decayed
 29 carbonatic materials of historical buildings. The reaction of DAP solutions with
 30 polycrystalline calcite of marbles is non-stoichiometric and forms a calcium phosphates
 31 mixture whose identification is tricky and controversial. This study investigated how the DAP
 32 molarity, the treatment method and the microstructure of the stone influence the formation of
 33 specific phases. Thermal treatments and cutting-edge techniques (XRD with synchrotron
 34 radiation in transmitting geometry and high resolution FTIR microspectroscopy) were used to
 35 overcome the analytical limits of the more conventional methods, shading light to an in depth
 36 evaluation of DAP consolidating processes and treatment conditions.

37 **Keywords**

38 Carrara marble; calcium phosphates; consolidation; diammonium hydrogenphosphate;
 39 synchrotron X-ray powder diffraction; high resolution FTIR microspectroscopy.

40

41

42

43 **Manuscript**

44 **1. Introduction**

45 Over the last few years, the use of diammonium hydrogenphosphate (DAP, $(\text{NH}_4)_2\text{HPO}_4$)
46 solutions has been introduced in the conservation field as a new inorganic-mineral treatments
47 to consolidate or protect carbonatic stone materials of historical monuments.

48 The DAP reaction with carbonatic substrates was investigated in terms of *i.e.*: compatibility
49 with the substrate [1], durability [2], resistance to simulated rain [3] or to phototrophic
50 colonization [4], desulfating agent [5,6].

51 The literature indicates that the reaction between DAP and calcite single crystals leads to the
52 formation of hydroxyapatite (HAP, $\text{Ca}_5(\text{PO}_4)_3\text{OH}$) [7,8], a stable and insoluble phase (K_{sp} 25
53 °C: calcite 4.8×10^{-9} mol/L, hydroxyapatite 1.6×10^{-117} mol/L [9]). More complex is its
54 reaction with carbonatic stones, because in this case it is non-stoichiometric and determines
55 the formation of a mixture of phases with a different Ca/P molar ratio [10–12]. The detected
56 phases after DAP treatments on carbonatic stone substrates are DCPD (brushite,
57 $\text{CaHPO}_4 \cdot 2\text{H}_2\text{O}$) [9,10], MCPM (monocalcium phosphate monohydrate, $\text{Ca}(\text{HPO}_4)_2 \cdot \text{H}_2\text{O}$) [5],
58 ACP (amorphous calcium phosphate, $\text{Ca}_x\text{H}_y(\text{PO}_4)_z \cdot n\text{H}_2\text{O}$ with $n = 3\text{--}4.5$) [10], MCPA
59 (monocalcium phosphate anhydrous, $\text{Ca}(\text{HPO}_4)_2$), TCP (tricalcium phosphate, $\text{Ca}_3(\text{PO}_4)_2$) and
60 OCP (octacalcium phosphate, $\text{Ca}_8(\text{HPO}_4)_2 \cdot 5\text{H}_2\text{O}$) [10,13]. However, Karampas &
61 Kontoyannis [14] and C. Drouet [15] reported that the straightforward characterization of
62 calcium phosphate phases is challenging due to the limits of a conventional analytical
63 approach; as a consequence, they highlighted the need of new analytical protocols. In
64 particular, one of the most critical issue is to define the most suitable method able to
65 distinguish HAP from OCP, especially if they are poorly crystalline or crystallize in a mixture

66 [14,15]. The structure of OCP consists of apatite-like layers alternated with hydrated layers
67 parallel to (100), deeply similar to HAP crystalline arrangement [16]; thus both of them give
68 rise to severe overlapping of X-ray diffraction peaks and vibrational bands.

69 DAP treatments can be performed without the addition of calcium ions or with an external
70 calcium source by adding calcium soluble salts [10,17,18]. The first method imply a slow
71 reaction with the substrate, which ideally favours a higher diffusion inside the substrate. The
72 formation of phases depends on the specific surface area of calcite grains and the descending
73 reactivity. The core idea of the second approach is to use calcium ions immediately available
74 for the reaction, accelerating the formation of calcium phosphates and resulting in the quicker
75 coverage of the marble surface with a film formation [17].

76 Despite the high number of studies on the crystallization of calcium phosphates and their
77 formation on the surface of carbonatic substrates, only a few studies [10,19,20] explored the
78 formation of calcium phosphate phases on marbles treated with DAP and using calcite of the
79 substrate as unique source for calcium ions.

80 For these reasons, the goal of this research is to determine how the crystallization of calcium
81 phosphates on Carrara marble after DAP consolidating treatments is influenced by the stone
82 substrate (micro-structural variations due to the conservation state) and by the treatment
83 method (application technique and DAP solution molarity) without using a further calcium
84 source. In this study, a set of quarried and decayed Carrara marble specimens were treated
85 with different method using DAP solutions of different molarities. Commercial powders of
86 calcium phosphates were used as references; OCP, a metastable phase not available for sale,
87 was synthesized and the structure of the obtained poly-crystalline material was refined by the
88 Rietveld method using high quality X-ray synchrotron powder diffraction data. To
89 unambiguously characterize the formation of newly-formed phosphate phases with similar
90 crystalline structure in multi-phase mixture and their arrangement on the marble surface, an

91 *ad hoc* multi-analytical approach was developed combining conventional and cutting-edge
92 techniques (XRD with synchrotron radiation in transmitting geometry, high resolution FTIR
93 microspectroscopy). Moreover, thermal treatments were performed to unequivocally
94 demonstrate the presence of the newly-formed HAP, overcoming the analytical limits of the
95 more conventional methods.

96

97 **2. Materials and methods**

98 *2.1. Materials*

99 The study was performed on prismatic specimens (5x5x2 cm) of quarried white Carrara
100 marble (a compact metamorphic carbonatic stone with homogeneous texture and
101 composition); part of them was artificially decayed (heating ramp up to 200 °C for 3 hours),
102 in order to induce micro-structural variations and grain detachment and to simulate naturally
103 weathered marbles.

104 DCPD (CAS Number 7789-77-7, assay \geq 98.0%, reagent grade), HAP (CAS Number 1306-
105 06-5, reagent grade), DAP (CAS Number 7783-28-0, assay \geq 99.0%, reagent grade) were
106 purchased by Sigma-Aldrich.

107 OCP, not available on sale, was synthesised at our laboratory, with a modified LeGeros
108 procedure [21]. The reagents for OCP synthesis were purchased by Merck, Darmstadt
109 Germany: $\text{NaH}_2\text{PO}_4 \cdot \text{H}_2\text{O}$ (CAS Number 10049-21-5, assay \geq 99.0%, reagent grade),
110 $\text{Ca}(\text{CH}_3\text{COO})_2 \cdot x\text{H}_2\text{O}$ (CAS Number 62-54-4, assay \geq 99.0%, reagent grade), HCl. 250 mL of
111 0.04 mol/L $\text{NaH}_2\text{PO}_4 \cdot \text{H}_2\text{O}$ (pH adjusted at 4.50 by the addition of 6.45 mL of 1 mol/L HCl
112 solution) were added drop wise with a speed of 1.39 mL/min in quiescent 250 mL of 0.04
113 mol/L $\text{Ca}(\text{CH}_3\text{COO})_2 \cdot x\text{H}_2\text{O}$ at 70 °C (\pm 1°C). At the end of the reaction, the pH was 4.28. The
114 solid precipitated was kept in contact with the mother solution for 20 minutes; after that, it

115 was isolated by filtration, rinsed with deionised water and dried at room temperature. The
116 nature of the precipitate was checked with a structure refinement by the Rietveld method
117 using the X-ray synchrotron powder diffraction pattern (further details in the section 2.2.2).
118 The high-quality refinement ($R(F^2) = 0.0435$, $wRp = 0.0588$) confirmed the formation of
119 monophasic OCP with a triclinic structure (space group: $P-1$), with unit-cell parameters: $a =$
120 $19.677(5) \text{ \AA}$, $b = 9.533(3) \text{ \AA}$, $c = 6.835(2) \text{ \AA}$, $\alpha = 90.14(3)^\circ$, $\beta = 92.55(4)^\circ$, $\gamma = 108.31(3)^\circ$, V
121 $= 1215.7(4) \text{ \AA}^3$, in good agreement with the data previously reported in the literature [16,22].

122 The marble specimens were treated by poultice and capillarity with two different molarities
123 (0.76 M and 3.00 M) of DAP aqueous solutions. The 0.76 M concentration corresponds to a
124 10% w/w and it was selected on the basis of previous experiments [10] and on the *in situ* DAP
125 consolidating practice [23]; the choice to include also 3.00 M concentration was suggested by
126 the literature [13], where this value was used to obtain the formation of a thicker layer of
127 calcium phosphates. After 24 hours, the treatments were removed and the specimens were left
128 drying at room temperature for 24 hours; at complete drying, the specimens were rinsed twice
129 by immersion in MilliQ water and dried again.

130

131 2.2. Methods

132 2.2.1. Scanning electron microscopy coupled with energy dispersive X-ray spectrometry

133 Morphological investigations of the newly-formed phases formed on marble were performed
134 in low and high vacuum mode by JEOL 5910 LV scanning electron microscope (SEM)
135 coupled with energy dispersive X-ray spectrometer (EDS) IXRF-2000 (0–20 keV). The shape
136 of newly-formed crystalline phases has been investigated by zenithal observations of the
137 surface of treated specimens; the growth of the phases from the surface, the action of the

138 treatment on calcite and the arrangement of the new phases on the substrate have been
139 analysed on cross sections.

140

141 2.2.2. X-ray powder diffraction techniques

142 The XRD pattern of references (commercial calcium phosphates and Carrara marble) were
143 investigated in Bragg-Brentano geometry with a Panalytical X'Pert PRO X-ray powder
144 diffractometer (XRD), equipped with a Cu-K α radiation source ($\lambda \sim 1.54 \text{ \AA}$), a PW 3050/60
145 goniometer, anti-scatter slit and divergence slit (1° and $1/2^\circ$ respectively), a PW3040/60
146 generator and a X'Celerator solid state detector PW3015/20 nickel filtered. The accelerating
147 voltage and electric current at the Cu anode were set to 40 kV and 40mA, respectively.
148 Powdered samples were finely ground and spread on zero background holders. Diffraction
149 data were collected at room temperature (rT, 25 °C) and after heating treatments (250 °C and
150 850 °C) in the angular range 3° – 75° 2θ , with a stepsize of 0.17° and scan-step time of 21.32 s.

151 The X-ray diffraction patterns of synthesized OCP and of calcium phosphates formed after
152 DAP treatments were collected at the ELETTRA Synchrotron facility, Trieste (Italy) in order
153 to investigate the presence of minor phases and to discriminate slight differences between
154 similar crystalline structures. The experiments were performed in transmission mode at the:

155 - XRD1 beamline [24]: measurements of the synthesized OCP. The diffraction data
156 were collected with a monochromatic wavelength of $\lambda = 0.700784(6) \text{ \AA}$, using a
157 Pilatus 2M hybrid-pixel area detector at rT and after heating treatments (250 °C and
158 850 °C). The investigation of the synthesized OCP with a synchrotron radiation was
159 required to: i) perform a structural refinement by the Rietveld method; ii) assess the
160 absence of apatite, as minor phase, and consequently to validate the synthesis route;

161 iii) investigate the phase transformation induced by heating and detect low fraction or
162 secondary phases as thermal by-products.
163 - MCX beamline [25]: measurements of calcium phosphates formed after DAP
164 treatments scratched from the marble surface. In-situ diffraction data were collected
165 with the high-resolution four circles Huber diffractometer from rT to 900 °C using a
166 gas blower (Oxford Danfysik DGB-0002) with a heating ramp speed of 5 °C/min, to
167 investigate the phase transformation in response to heating. The X-ray diffraction
168 patterns were collected at specific temperatures where phase transitions are expected
169 (250 °C, 750 °C, 850 °C). Additional patterns were collected at 100 °C, 500 °C, at 900
170 °C and after cooling to rT. The diffraction patterns were collected using a focalized
171 monochromatic beam of $\lambda = 0.885227(6) \text{ \AA}$ in the 2θ angular range of $1.5 - 50^\circ$, with
172 a step size of 0.01° .

173 A whole pattern profile fitting of the diffraction data was performed by the Rietveld method,
174 using the GSAS package (<http://www.ccp14.ac.uk/solution/gsas/>; profile function: pseudo-
175 Voigt, background function: Chebyshev polynomial).

176 2.2.3. *High resolution ATR-FTIR microspectroscopy*

177 ATR μ FT-IR measurements of calcium phosphates were carried out in order to investigate the
178 microscale distribution of crystalline phases with a LUMOS standalone FT-IR microscope
179 (Bruker OptikGmbH), equipped with a motorized XYZ sample stage and automated Ge-ATR
180 probe (tip diameter about 100 μm), driven by a piezo, included into the 8x cassegrain
181 objective (NA = 0.6). Considering the Ge refractive index value (4), the theoretical lateral
182 resolution of about 1 μm [26] was obtained collecting the spectra with a $4.0 \times 4.0 \mu\text{m}^2$
183 aperture, step size (along x and y) around 3.5 μm , 16 or 32 scans and different ATR pressure
184 (low, medium, high). The data were treated with the OPUS-IR™ software (Bruker Optik
185 GmbH, version 7.5).

186

187 **3. Results and discussion**

188 *3.1 Analysis of the newly-formed phases*

189 After DAP treatments, the surfaces of all the specimens show the formation of calcium
190 phosphates (Ca and P clearly detected by EDS) with different morphologies (rose-like with
191 irregular contours, spherical units or aggregates of spherical units in elongated arrangements,
192 plate-like blades) arranged in a *shell* around calcite grains and between grain boundaries.
193 Moreover, some specimens exhibit further calcium phosphate crystals grown over the *shell*.
194 Here, the *shell* and the calcium phosphate crystallized over the *shell* are called “*newly-formed*
195 *system*” (Fig. 1a-1d).

196 In all the specimens, the XRD patterns of the *shell*, collected with a conventional instrument
197 and by using a synchrotron radiation to improve the signal intensity, show the characteristic
198 Bragg peaks of OCP in mixture with calcite (Fig. 2a and Fig. 2b). The XRD peaks of calcite
199 are due to the presence of calcite grains detached during the treatment and embedded in the
200 *shell*, as shown in Fig. 1b. The XRD peaks of OCP at 18.56 Å (d_{100}), 9.36 Å, 9.03 Å and 5.49
201 Å are broad, weak and with relative intensities slightly different from the synthesized
202 reference material, suggesting that this phase is probably formed as sub-micrometric crystals
203 or contains structural defects and vacancies. The presence of HAP in these XRD patterns is
204 ambiguous. Two peaks, corresponding to inter-planar distances of 3.42 Å and 1.71 Å
205 (indicated in Fig. 2a by the dotted lines), could be attributed to HAP. However, the severe
206 overlap of OCP and HAP diffraction patterns (due to the close relationship between the two
207 structures) prevents the univocal identification of HAP.

208 The spectra acquired by high resolution ATR-FTIR microspectroscopy of references powders
209 of OCP and HAP permit to clearly distinguish the two phases by the characteristic vibrations

210 in the fingerprint region of PO_4^{2-} groups [27] and HPO_4^{2-} groups [28–30]. However, even
211 with this technique, it is not possible to unequivocally identify HAP in the *shell* because all
212 the acquired spectra reveal hybrid vibrational patterns between HAP and OCP that can be
213 considered the convolution of vibrational features of the two phases (Fig. 3a and Fig. 3b,
214 spectrum 1 and 2); this ambiguity persists down to the microscale, as demonstrated by the
215 spectra collected on areas of $1 \times 1 \mu\text{m}^2$. These findings indicate that OCP and the not well
216 defined apatites are not formed as single, crystalline, micrometric individuals but, instead,
217 they are most likely formed as sub-micrometric multiphase mixture. Furthermore, the
218 detection of CO_3^{2-} vibrational bands at 1460 cm^{-1} , 1399 cm^{-1} and 868 cm^{-1} suggest the
219 formation of carbonate-substituted non-stoichiometric apatite, with the typical surface layers
220 hosting groups such as CO_3^{2-} , HPO_4^{2-} instead of PO_4^{3-} [27,31]. Therefore, the *shell* consists by
221 a complex mixture of sub-micrometric non-stoichiometric phases due to their nucleation in a
222 not ideal reaction environment.

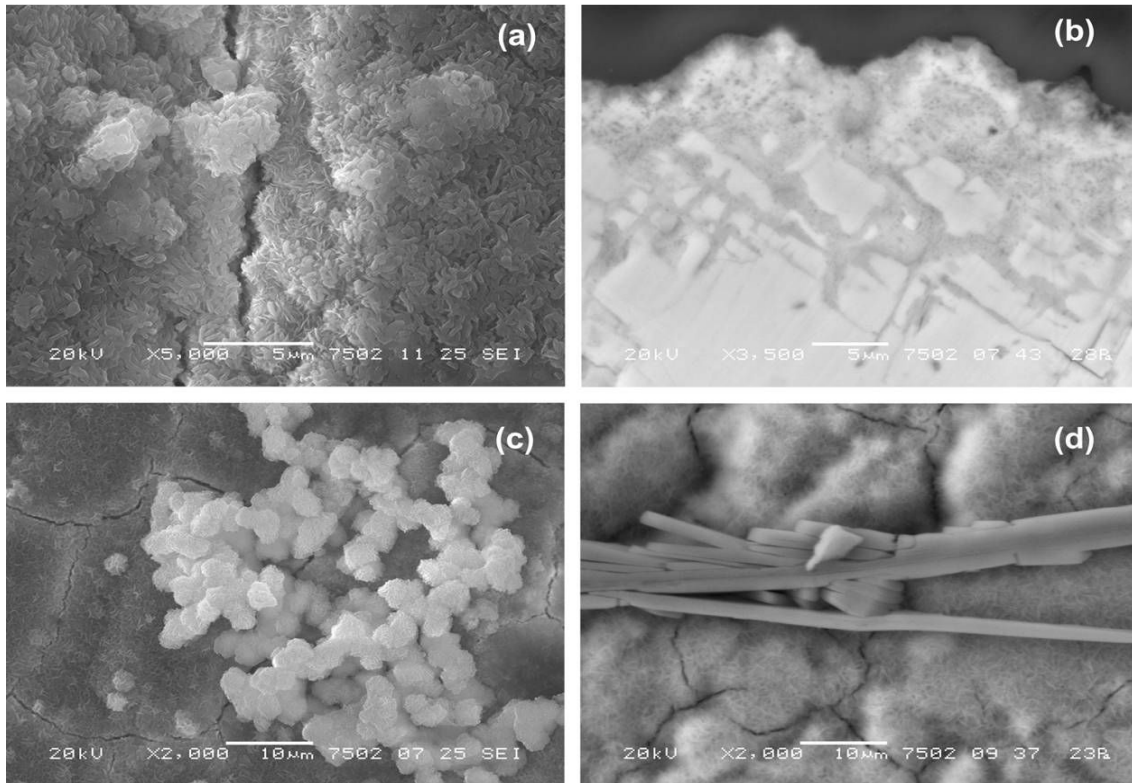
223 Over the *shell*, the composition of newly-formed phases depends on the molarity of the
224 solution. In fact, after 3.00 M DAP treatments, spherical aggregates of thin, rose-like blades
225 are formed over the *shell* and they are composed of OCP, calcite and ambiguous HAP (Fig.
226 1c, Fig. 2a and Fig. 2b). Instead, the 0.76 M DAP solutions form acicular plate-like crystals
227 (Fig. 1d) heterogeneously distributed over the *shell*; these crystals are composed of DCPD, as
228 clearly identified with high resolution ATR-FTIR microspectroscopy by the marker HPO_4^{2-}
229 vibrations at 1125 cm^{-1} , 1051 cm^{-1} , 985 cm^{-1} [14,27] (Fig. 3a and Fig. 3b, spectrum 3) and
230 confirmed by a very weak XRD peak (Fig. 2a and Fig. 2b).

231 DCPD is an acid calcium phosphates, it has a Ca/P molar ratio of 1.00 and its growth is most
232 likely due to two simultaneous factors: the Ca/P molar ratio [5,32] and the decrease of pH of
233 the solution. Its nucleation requires the availability of HPO_4^{2-} groups and a low Ca^{2+}
234 concentration. The DAP speciation in water leads to the formation of a much higher amount

235 of HPO_4^{2-} ions, compared to PO_4^{3-} ions [20], therefore its formation seems to be favoured
236 during the reaction, alongside HAP. Actually, its crystallization also requires an acidification
237 of the solution, conditions not suitable for the formation of OCP and HAP. Such reaction
238 conditions probably occur in the final steps of the reaction of 0.76 M DAP solutions, when the
239 pH decreases, due to the release of H^+ from the reagent speciation, and slows the HAP and
240 OCP formation (phases preferentially formed under basic or neutral conditions [11]). The
241 decrease of pH, combined to the crystallization of OCP and HAP (which consume Ca^{2+} and
242 PO_4^{3-} ions), actually favours the formation of DCPD. At the same time, the growth of the *shell*
243 starts to represent a barrier for the release of further Ca^{2+} ions from the marble substrate,
244 which further inhibit the formation of phases with high Ca/P molar ratio. Moreover, since the
245 0.76 M DAP solutions have a “reduced capability” to dissolve Ca^{2+} ions, the treatments with
246 this molarity are definitely less aggressive on the stone substrate and, for this reason, the *shell*
247 is well adherent to the substrate. On the contrary, since 3.00 M DAP solutions dissolve a high
248 amounts of Ca^{2+} ions from the substrate, these treatments are more aggressive on the
249 substrate, calcite shows deep corrosion marks and the *shell*, thicker than those of 0.76 M
250 solutions, is evidently detached from the substrate.

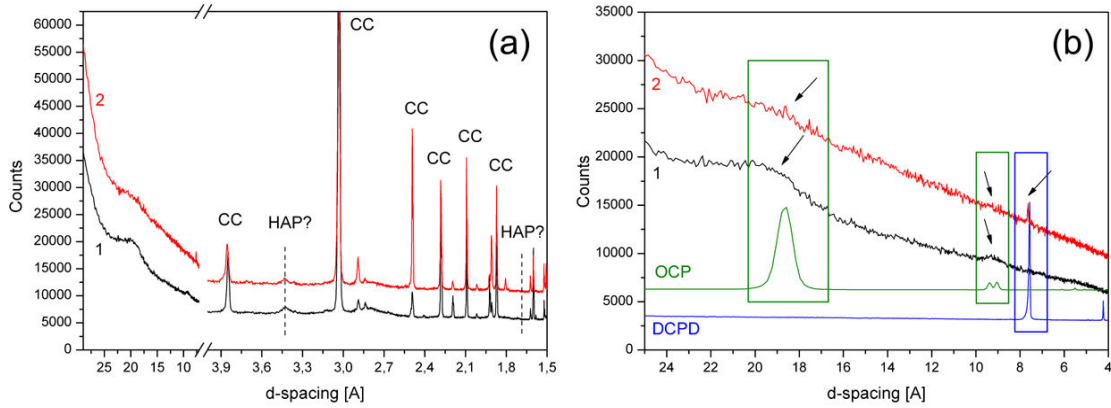
251 The thickness of the *newly-formed system*, as demonstrated by measurements carried out on
252 polished cross sections, is strongly influenced by the treatment methods. In fact, poultice and
253 capillarity are characterized by a different contact at the interface between the marble and the
254 thickener (either cellulose pulp or paper filter): the cellulose pulp provides a continuous
255 contact not allowing a “free growth” of calcium phosphate crystals; for this reason the *newly-*
256 *formed system* is thin (2-10 μm). On the contrary, with capillarity the contact shows several
257 vacancies determining the occurrence of gaps with a certain amount of free solution without
258 spatial limitations. As a consequence, the *newly-formed system* is thicker (10-20 μm).

259 The stone microstructure influences the thickness of the *newly-formed system* as well. The
260 decohesion of weathered substrates determines a higher porosity, and consequently higher
261 specific surface area and reaction rate; therefore the *newly-formed system* is slightly thicker
262 for decayed specimens.



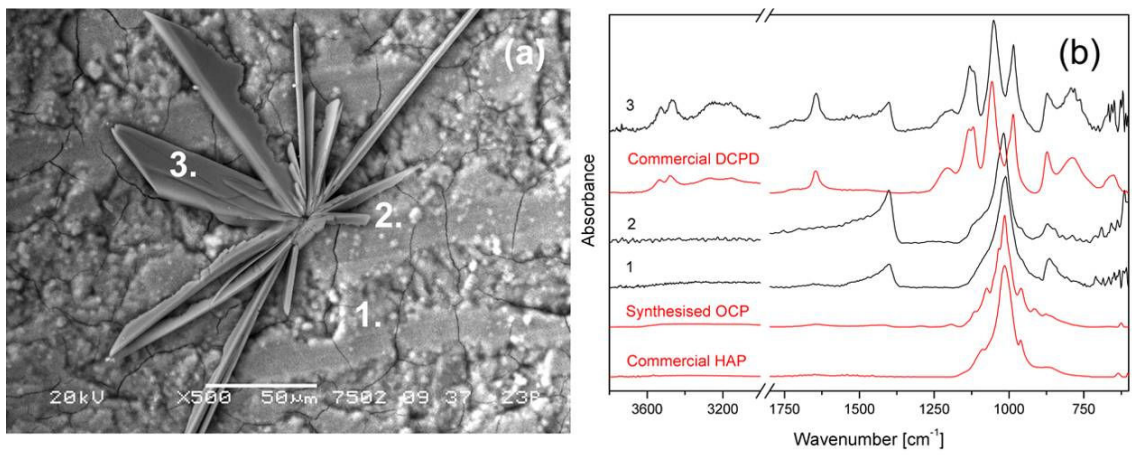
263

264 **Fig. 1.** SEM images of calcium phosphates formed after DAP treatments: (a) surface of marble showing the
265 newly-formed calcium phosphate phases after 3.00 M DAP treatment; (b) polished cross section of calcium
266 phosphates *newly-formed system* which embeds calcite grains detached during the 3.00 M DAP treatment; (c)
267 spherical structures formed over the *shell* after 3.00 M DAP treatments; (d) acicular plate-like crystals formed
268 over the *shell* after 0.76 M DAP treatments.



269

270 **Fig. 2.** XRD patterns of calcium phosphates formed on specimens treated by 3.00 M (pattern 1) and 0.76 M
 271 (pattern 2) DAP solutions: (a) calcite peaks (CC) embedded in the calcium phosphate *shell* and peaks compatible
 272 with HAP (dotted lines); (b) formation of OCP and a mixture of OCP and DCPD.



273

274 **Fig. 3.** (a) SEM image of the *newly-formed system*; (b) FTIR spectra of the calcium phosphates *shell* (spectra 1
 275 and 2) and DCPD acicular platelets in characteristic anisotropic plate-like aggregates (spectrum 3) crystallised
 276 over the *shell* after 0.76 M DAP treatments.

277

278 *3.2 Confirm of HAP formation by thermal treatments*

279 OCP has been described as a precursor in the formation of HAP [33] and it is highly likely
 280 that OCP acts as growth seeds on the calcite grains for the nucleation of HAP.

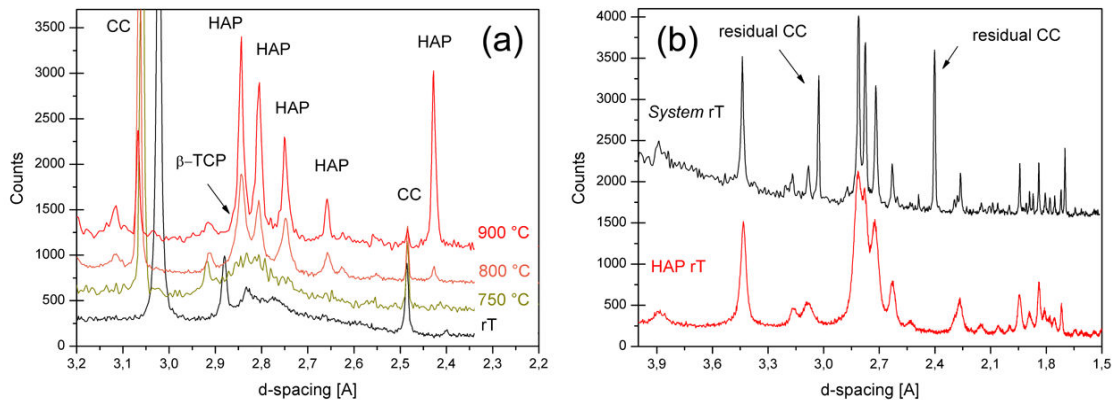
281 For this reason, a set of thermal treatments were carried out to demonstrate the presence of
282 HAP in the *newly-formed system* since heating is proved to be an effective approach to
283 discriminate phases which exhibit similar crystalline structure at room conditions
284 [14,30,34,35]. This procedure was performed first on references and then on the calcium
285 phosphates of the *newly-formed system*.

286 Heating of synthesized OCP at 250 °C leads to the first phase transition with the formation of
287 an amorphous phase. The OCP main transformation occurs after heating at 850 °C, when the
288 amorphous-apatite/collapsed-OCP is completely transformed into a mixture of β -TCP (β -
289 $\text{Ca}_3(\text{PO}_4)_2$) and β -CPP (β - $\text{Ca}_2\text{P}_2\text{O}_7$) [30,35,36]. The calculated ratio of the phases, as resulted
290 from the Rietveld refinement, is: 66.8 wt % and 33.2 wt % of β -TCP and β -CPP respectively,
291 in agreement with literature data [30]; these findings basically validated the synthesis route.

292 Heating of commercial HAP showed no detectable phase changes until 750 °C; from 850 °C
293 the XRD and FTIR spectra revealed the formation of very sharp peaks of β -TCP and HAP
294 [14,34,37], with β -TCP predominant respect to HAP. The growth of sharp peaks is due to the
295 increase, with heating, of the crystallinity degree of poorly-crystalline HAP, while the
296 formation of β -TCP is due to the presence of “impurities”, such as HPO_4^{2-} or CO_3^{2-} in the
297 commercial HAP. The formation of a relevant amount of β -TCP indicates that this reference
298 material is poorly-crystalline and non-stoichiometric. On the contrary, the heating of poorly-
299 crystalline stoichiometric HAP should not produce any heating by-product (*i.e.* β -TCP) but
300 only the increase of the crystallinity degree [14,37]. For the characterization of the *newly-*
301 *formed system*, the XRD peaks corresponding to the d spacing of 2.81 Å, 2.77 Å, 2.71 Å and
302 2.62 Å were used as HAP markers as they do not present significant superimposition with
303 other phases.

304 Since the references showed that the main transformation occurred at 850 °C, the following
305 discussion focuses on the phase transformation occurred above 850 °C.

306 Fig. 4a shows the pattern of thermal treatments performed on a *newly-formed system* and it is
 307 representative of the results obtained in all the specimens. In the range between 850 °C and
 308 900 °C, the broad weak band between 2.90 Å and 2.62 Å changes into a sequence of sharper,
 309 well-defined peaks centred at 2.84 Å, 2.80 Å, 2.75 Å and 2.65 Å. These peaks, as well as the
 310 sharper peaks at 8.22 Å, 3.47 Å and 2.28 Å, are unambiguously attributed to the crystallinity
 311 increase of HAP above 850°C that minimizes the overlap with the other phases. Therefore,
 312 the initial presence in the *newly-formed system* of nano-crystalline non-stoichiometric HAP is
 313 definitely confirmed in every specimen (Fig. 4b). The formation of β -TCP is documented by
 314 the peaks at 3.20 Å, 2.86 Å, 2.33 Å, 2.15 Å and 2.03 Å, even though they are very weak. β -
 315 TCP is the transformation product of both OCP and non-stoichiometric apatite, and after
 316 heating of the *newly-formed system* it is rather scarce; these data indicate that in the original
 317 *newly-formed system* i) OCP and non-stoichiometric apatite (such as carbonate-substituted
 318 apatite detected by FTIR) were only minor phases; ii) HAP, the main phase, was mainly
 319 poorly-crystalline or nano-crystalline but stoichiometric.



320

321 **Fig. 4.** XRD patterns of the calcium phosphate *newly-formed system*: (a) acquired *in-situ* during the thermal
 322 treatments, showing the transformation of the broad band between 2.90 Å and 2.62 Å into a sequence of sharper,
 323 well-defined peaks of HAP centred at 2.84 Å, 2.80 Å, 2.75 Å and 2.65 Å. Weak β -TCP peaks and peaks of
 324 residual calcite (CC) are also present; (b) comparison of the heated *newly-formed system* after cooling to rT and
 325 commercial HAP.

326 4. Conclusions

327 The nature and the arrangement of the newly-formed phases after DAP treatment on Carrara
328 marble were properly characterized through the development of a comprehensive multi-
329 analytical approach. X-ray diffraction with synchrotron light in transmitting geometry and
330 thermal treatments were used to investigate the presence of HAP overcoming some analytical
331 limits of the more conventional methods. The potentialities of high lateral resolution ATR-
332 FTIR microspectroscopy have been assessed for the unambiguous identification of DCPD and
333 minor phases (*i.e.* carbonate-substituted apatite).

334 The experimental findings of this study clearly showed that DAP consolidating treatments
335 performed on massive Carrara marble specimens form a *newly-formed system* of calcium
336 phosphates that depends on the DAP molarity, the treatment method and the microstructure of
337 the substrate. In general, the composition and the localization of the phases, as well as the
338 thickness of the *newly-formed system*, directly depend on the availability of free Ca^{2+} ions and
339 on the reaction kinetics.

340 The formation of hydroxyapatite in a poorly-crystalline or nano-crystalline stoichiometric
341 form is unambiguously demonstrated by thermal treatments. OCP, non-stoichiometric apatite
342 and DCPD are only minor phases.

343 From the conservation point of view, even though DCPD is more soluble than HAP and OCP,
344 its formation in heterogeneously distributed aggregates is highly positive because: i) it can be
345 considered a further sacrificial phase for the protection of the treated surfaces from
346 environmental agents; ii) DCPD is a precursor in the formation of apatite and it tends to
347 transform into HAP by dissolution and re-precipitation processes; iii) the formation of DCPD
348 reflects a minor chemical attack on the substrate.

349

350 **Conflicts of interest**

351 The authors declare that there are no conflicts of interest to declare

352 **Declarations of interest**

353 None

354 **Funding sources**

355 This research did not receive any specific grant from funding agencies in the public,
356 commercial, or not-for-profit sectors.

357

358 **Acknowledgements**

359 The authors gratefully acknowledge the Elettra Synchrotron Trieste for allocation of
360 experimental beamtime and Dr. Elena Ferrari (Dipartimento di Scienze della Terra, Università
361 degli Studi di Milano) for her support during the optimization of the synthesis route of OCP.

362

363 **References**

364 [1] E. Sassoni, G. Graziani, E. Franzoni, An innovative phosphate-based consolidant for
365 limestone. Part 1: Effectiveness and compatibility in comparison with ethyl silicate,
366 Constr. Build. Mater. 102 (2016) 918–930. doi:10.1016/j.conbuildmat.2015.10.202.

367 [2] E. Sassoni, G. Graziani, E. Franzoni, An innovative phosphate-based consolidant for
368 limestone. Part 2: Durability in comparison with ethyl silicate, Constr. Build. Mater.
369 102 (2016) 931–942. doi:10.1016/j.conbuildmat.2015.10.202.

370 [3] G. Graziani, E. Sassoni, G.W. Scherer, E. Franzoni, Resistance to simulated rain of
371 hydroxyapatite- and calcium oxalate-based coatings for protection of marble against

- 372 corrosion, *Corros. Sci.* 127 (2017) 168–174. doi:10.1016/j.corsci.2017.08.020.
- 373 [4] B.C. Barriuso, G. Botticelli, O.A. Cuzman, I. Osticioli, P. Tiano, M. Matteini,
374 Conservation of calcareous stone monuments: Screening different diammonium
375 phosphate based formulations for countering phototrophic colonization, *J. Cult. Herit.*
376 27 (2017) 97–106. doi:10.1016/j.culher.2017.03.002.
- 377 [5] E. Molina, L. Rueda-Quero, D. Benavente, A. Burgos-Cara, E. Ruiz-Agudo, G.
378 Cultrone, Gypsum crust as a source of calcium for the consolidation of carbonate
379 stones using a calcium phosphate-based consolidant, *Constr. Build. Mater.* 143 (2017)
380 298–311. doi:10.1016/j.conbuildmat.2017.03.155.
- 381 [6] M. Matteini, C. Colombo, G. Botticelli, M. Casati, C. Conti, R. Negrotti, M. Realini,
382 E. Possenti, Ammonium phosphates to consolidate carbonatic stone materials: an
383 inorganic-mineral treatment greatly promising, in: *Built Herit. 2013 Monit. Conserv.*
384 *Manag.*, 2013: pp. 1278–1286.
- 385 [7] M. Ni, B.D. Ratner, Nacre surface transformation to hydroxyapatite in a phosphate
386 buffer solution., *Biomaterials.* 24 (2003) 4323–31. doi:10.1016/S0142-9612(03)00236-
387 9.
- 388 [8] A. Kasiotas, C. Perdikouri, C. V. Putnis, A. Putnis, Pseudomorphic replacement of
389 single calcium carbonate crystals by polycrystalline apatite, *Mineral. Mag.* 72 (2008)
390 77–80. doi:10.1180/minmag.2008.072.1.77.
- 391 [9] M. Matteini, S. Rescic, F. Fratini, G. Botticelli, Ammonium Phosphates as
392 Consolidating Agents for Carbonatic Stone Materials Used in Architecture and
393 Cultural Heritage: Preliminary Research, *Int. J. Archit. Herit. Conserv. Anal. Restor.* 5
394 (2011) 717–736. doi:10.1080/15583058.2010.495445.
- 395 [10] E. Possenti, C. Colombo, D. Bersani, M. Bertasa, A. Botteon, C. Conti, P.P. Lottici,
396 M. Realini, New insight on the interaction of diammonium hydrogenphosphate
397 conservation treatment with carbonatic substrates: A multi-analytical approach,

- 398 Microchem. J. 127 (2016) 79–86. doi:10.1016/j.microc.2016.02.008.
- 399 [11] L. Wang, G.H. Nancollas, Calcium Orthophosphates: Crystallization and Dissolution,
400 Chem. Rev. 108 (2008) 4628–4669. doi:10.1021/cr0782574.Calcium.
- 401 [12] S. V. Dorozhkin, Calcium orthophosphates, J. Mater. Sci. 42 (2007) 1061–1095.
402 doi:10.1007/s10853-006-1467-8.
- 403 [13] E. Sassoni, G. Graziani, E. Franzoni, Repair of sugaring marble by ammonium
404 phosphate: Comparison with ethyl silicate and ammonium oxalate and pilot application
405 to historic artifact, Mater. Des. 88 (2015) 1145–1157.
406 doi:10.1016/j.matdes.2015.09.101.
- 407 [14] I.A. Karampas, C.G. Kontoyannis, Characterization of calcium phosphates mixtures,
408 Vib. Spectrosc. 64 (2013) 126–133. doi:10.1016/j.vibspec.2012.11.003.
- 409 [15] C. Drouet, Apatite formation: Why it may not work as planned, and how to
410 conclusively identify apatite compounds, Biomed Res. Int. 2013 (2013) 1–12.
411 doi:10.1155/2013/490946.
- 412 [16] M. Mathew, W.E. Brown, L.W. Schroeder, B. Dickens, Crystal structure of
413 octacalcium bis(hydrogenphosphate) tetrakis(phosphate)pentahydrate,
414 $\text{Ca}_8(\text{HPO}_4)_2(\text{PO}_4)_4 \cdot 5\text{H}_2\text{O}$, J. Crystallogr. Spectrosc. Res. 18 (1988) 235–250.
415 doi:10.1007/BF01194315.
- 416 [17] E. Sassoni, Phosphate-based treatments for conservation of stone, RILEM Tech. Lett.
417 2 (2017) 14. doi:10.21809/rilemtechlett.2017.34.
- 418 [18] E. Sassoni, Hydroxyapatite and Other Calcium Phosphates for the Conservation of
419 Cultural Heritage: A Review, Materials (Basel). 11 (2018) 557.
420 doi:10.3390/ma11040557.
- 421 [19] M. Kamiya, J. Hatta, E. Shimada, Y. Ikuma, M. Yoshimura, H. Monma, AFM analysis
422 of initial stage of reaction between calcite and phosphate, Mater. Sci. Eng. B. 111
423 (2004) 226–231. doi:10.1016/j.mseb.2004.05.007.

- 424 [20] S. Naidu, G.W. Scherer, Nucleation, growth and evolution of calcium phosphate films
425 on calcite, *J. Colloid Interface Sci.* 435 (2014) 128–137.
426 doi:10.1016/j.jcis.2014.08.018.
- 427 [21] R.Z. LeGeros, Preparation of octacalcium phosphate (OCP): A direct fast method,
428 *Calcif. Tissue Int.* 37 (1985) 194–197. doi:10.1007/BF02554841.
- 429 [22] W.E. Brown, J.P. Smith, J.R. Lehr, W.A. Frazier, Octacalcium Phosphate and
430 Hydroxyapatite: Crystallographic and Chemical Relations between Octacalcium
431 Phosphate and Hydroxyapatite, *Nature*. 196 (1962) 1050–1055.
432 doi:10.1038/1961050a0.
- 433 [23] D. Pittaluga, F. Fratini, A. Nielsen, S. Rescic, Industrial archaeological sites and
434 architectonic remains: the problem of consolidation in humid areas, in: *Arcadia*
435 *Ricerche* (Ed.), *Sci. E Beni Cult.* XXVIII, 2012: pp. 303–312.
- 436 [24] A. Lausi, M. Polentarutti, S. Onesti, J.R. Plaisier, E. Busetto, G. Bais, L. Barba, A.
437 Cassetta, G. Campi, D. Lamba, A. Pifferi, S.C. Mande, D.D. Sarma, S.M. Sharma, G.
438 Paolucci, Status of the crystallography beamlines at Elettra, *Eur. Phys. J. Plus.* 130
439 (2015) 43. doi:10.1140/epjp/i2015-15043-3.
- 440 [25] L. Rebuffi, J.R. Plaisier, M. Abdellatif, A. Lausi, P. Scardi, MCX: a Synchrotron
441 Radiation Beamline for X-ray Diffraction Line Profile Analysis, *Zeitschrift Für Anorg.*
442 *Und Allg. Chemie.* 640 (2014) 3100–3106. doi:10.1002/zaac.201400163.
- 443 [26] M. Bertasa, E. Possenti, A. Botteon, C. Conti, A. Sansonetti, R. Fontana, J. Striova, D.
444 Sali, Close to the diffraction limit in high resolution ATR FTIR mapping:
445 demonstration on micrometric multi-layered art systems, *Analyst.* 142 (2017) 4801–
446 4811. doi:10.1039/C7AN00873B.
- 447 [27] S. Koutsopoulos, Synthesis and characterization of hydroxyapatite crystals: a review
448 study on the analytical methods., *J. Biomed. Mater. Res.* 62 (2002) 600–12.
449 doi:10.1002/jbm.10280.

- 450 [28] B.O. Fowler, M. Markovic, W.E. Brown, Octacalcium phosphate. 3. Infrared and
451 Raman vibrational spectra, *Chem. Mater.* 5 (1993) 1417–1423.
452 doi:10.1021/cm00034a009.
- 453 [29] E.E. Berry, C.B. Baddiel, Some assignments in the infra-red spectrum of octacalcium
454 phosphate, *Spectrochim. Acta.* 23A (1967) 1781–1792. doi:10.1016/0584-
455 8539(67)80061-8.
- 456 [30] B.O. Fowler, E.C. Moreno, W.E. Brown, Infra-red spectra of hydroxyapatite,
457 octacalcium phosphate and pyrolysed octacalcium phosphate, *Arch. Oral Biol.* 11
458 (1966) 477–492. doi:10.1016/0003-9969(66)90154-3.
- 459 [31] Y. Lee, Y.M. Hahm, S. Matsuya, M. Nakagawa, K. Ishikawa, Characterization of
460 macroporous carbonate-substituted hydroxyapatite bodies prepared in different
461 phosphate solutions, *J. Mater. Sci.* 42 (2007) 7843–7849. doi:10.1007/s10853-007-
462 1629-3.
- 463 [32] E. Sassoni, G. Graziani, E. Franzoni, G.W. Scherer, Conversion of calcium sulfate
464 dihydrate into calcium phosphates as a route for conservation of gypsum stuccoes and
465 sulfated marble, *Constr. Build. Mater.* 170 (2018) 290–301.
466 doi:10.1016/j.conbuildmat.2018.03.075.
- 467 [33] Y.-H. Tseng, C.-Y. Mou, J.C.C. Chan, Solid-state NMR study of the transformation of
468 octacalcium phosphate to hydroxyapatite: a mechanistic model for central dark line
469 formation., *J. Am. Chem. Soc.* 128 (2006) 6909–18. doi:10.1021/ja060336u.
- 470 [34] J.C. Elliott, Hydroxyapatite and Nonstoichiometric Apatites, in: *Struct. Chem. Apatites*
471 *Other Calcium Orthophosphates*, 1994: pp. 111–189. doi:10.1016/B978-0-444-81582-
472 8.50008-0.
- 473 [35] J.C. Elliott, General Chemistry of the Calcium Orthophosphates, in: *Struct. Chem.*
474 *Apatites Other Calcium Orthophosphates*, 1994: pp. 1–62. doi:10.1016/B978-0-444-
475 81582-8.50006-7.

- 476 [36] A. Massita, A. El Yacoubi, B.C. El Idrissi, K. Yamni, Synthesis and characterization
477 of nano-sized β -Tricalcium phosphate: Effects of the aging time, *J. Appl. Chem.* 7
478 (2014) 57–61. [http://www.iosrjournals.org/iosr-jac/papers/vol7-issue7/Version-](http://www.iosrjournals.org/iosr-jac/papers/vol7-issue7/Version-1/J07715761.pdf)
479 [1/J07715761.pdf](http://www.iosrjournals.org/iosr-jac/papers/vol7-issue7/Version-1/J07715761.pdf).
- 480 [37] S.N. Danilchenko, A. V. Koropov, I.Y. Protsenko, B. Sulkiö-Cleff, L.F. Sukhodub,
481 Thermal behavior of biogenic apatite crystals in bone: An X-ray diffraction study,
482 *Cryst. Res. Technol.* 41 (2006) 268–275. doi:10.1002/crat.200510572.
- 483